Plasma Sources Sci. Technol. 3 (1994) 418–425. Printed in the UK

Spatial distributions of dust particles in plasmas generated by capacitively coupled radiofrequency discharges

Seung J Choi†, Peter L G Ventzek‡, Robert J Hoekstra and Mark J Kushner§

Department of Electrical and Computer Engineering, University of Illinois, 1406 W. Green St, Urbana, IL 61801, USA

Abstract. The transport of particles ('dust') in low-pressure electrical glow discharges is of interest with respect to contamination of semiconductor wafers during plasma etching and deposition. The distribution of dust particles in these reactors is determined by a variety of forces, the most important being electrostatic, viscous ion drag, gravitational, thermophoretic and neutral fluid drag. In this paper we present results from a series of computer models to predict the spatial distribution of dust particles in capacitively coupled electrical glow discharges considering these forces. The results are parametrized over power deposition, gas flow and particle size. We find that the spatial distribution of dust depends on the spatial dependence of the sheaths and plasma potential in bulk plasma which in turn depend upon the electrical topography of the surfaces. Experimentally observed 'dome' and 'ring' distributions of dust particles are computationally reproduced for specific combinations of discharge power particle size and substrate topography.

I. Introduction

Particulates ('dust' particles) are common contaminants in low-pressure (< hundreds of mTorr), partially ionized (electron density 10^9–$10^{11}\,cm^{-3}$) plasma processing electrical glow discharges for semiconductor etching and deposition [1–10]. The dust particles negatively charge, and particles of a few micrometres in size have hundreds to thousands of elementary charges [11, 12]. Dust particles generally accumulate in specific regions of the radio frequency (RF) discharges which are commonly used in plasma processing. Roth *et al* first used laser light scattering to observe that particles accumulate near the bulk plasma–sheath boundary in these discharges [1], as was later confirmed by Selwyn *et al* [2–4], Jellum *et al* [5–7], and Watanabe *et al* [8, 9]. Large particles ($>0.1\,\mu m$) accumulate near the sheath edge, while small particles accumulate in the centre of the discharge at the location of the maximum in the plasma potential. Selwyn *et al* [3] and Carlile *et al* [10] also observed that particles accumulated in rings around and domes above the semiconductor wafers in reactive ion etching (RIE) discharges.

Sommerer *et al* [13] and Barnes *et al* [14] proposed that transport of small particles (when gravity is not important) is dominated by two forces: electrostatic and viscous ion drag. The former force accelerates negatively charged particles towards the centre of electropositive plasmas or towards local maxima in the plasma potential. The latter force accelerates particles in the direction of net ion flux, which is generally towards the boundaries of the plasma. (The ion drag force results from orbits of positive ions around the dust particle which transfer momentum to the particle in the direction of the net ion flux [11, 12]. These forces have also been theoretically addressed by Graves *et al* [15, 16] and computationally addressed by Choi and Kushner [11, 12].

The details of the geometry of the reactor are important in determining the location at which particles accumulate in RF discharges. For example, for large particles, the electrostatic and ion drag forces balance near the edge of the sheath. The electrical topography of the substrate, which determines the shape of the sheath, is therefore important in determining the distribution of dust particles. Viscous fluid forces accelerate particles in the direction of the gas flow. The flow field through nozzles and around obstacles is therefore important with respect to dust distributions. The geometry of the reactor can also determine the temperature field, which generates thermophoretic forces [17].

The importance of the electrical topography of the substrates in determining the distribution of dust has been noted by the experimental observations that dust often accumulates in rings and domes above semiconductor wafers [18]. Selwyn *et al* [3] also observed that particles accumulate in the centre of metallic washers placed on the electrode and in grooves surrounding the wafer in RF discharges. These observations are presumably explained by the perturbing effects of these topographies on the potential profile and ion fluxes. Further

† Present address: Sandia National Laboratory, Albuquerque, NM 87185, USA.
‡ Present address: Hokkaido University, Department of Electrical Engineering, Sapporo 060, Japan.
§ Author to whom correspondence should be addressed.

0963-0252/94/030418 + 08$19.50

evidence for the importance of the electrical topography in determining dust distributions can be found with recent electric probe measurements of the plasma potential in RF discharges. These measurements showed that particles are commonly found in the vicinity of positive potential traps (perhaps as large as 7 V) at the edges of wafers [10, 18].

To predict the accumulation of particles in RF discharges one must therefore self-consistently account for the shielding and charging of particles in the plasma, the ion flux which provides the ion drag forces, the electric field which generates the electrostatic force, the fluid flow field which provides the viscous drag force and the temperature field which generates thermophoretic forces. A series of computer models has been developed to predict the dynamics of the motion of dust particles in capacitively coupled RF discharges considering these forces. The models are described in section 2 followed by a discussion of our results in section 3. Our concluding remarks are presented in section 4.

2. Description of the model

The model we have used in this study is a series of five linked simulations, schematically shown in figure 1. The first model is a pseudoparticle in cell simulation (PICS) which provides the electrical charges on the dust particle and ion–dust momentum transfer cross sections [11, 12]. The second is a two-dimensional Monte Carlo–fluid hybrid (MCFH) model for plasma properties of RF discharges [19]. The third is a two-dimensional plasma chemistry Monte Carlo simulation (PCMCS) which provides ion velocity distributions [19]. The fourth is an advective flow field model. The fifth is the dust particle transport (DPT) model which is the module in which the dust particle trajectories are actually computed. (To avoid confusion, computational particles in a PICS or MCS will be called pseudoparticles; contaminating particulates in the plasma will be called dust particles.)

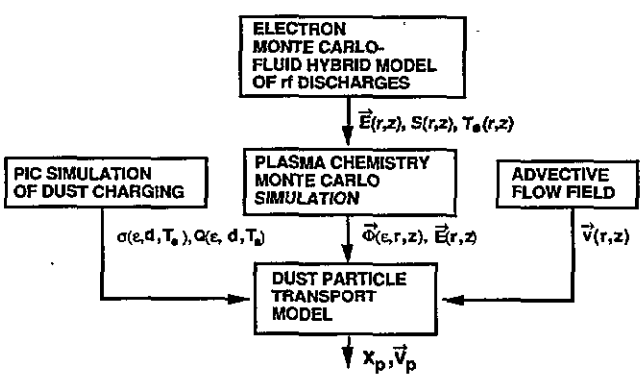

Figure 1. Schema of the model for particle trapping. Results from a Monte Carlo–fluid hybrid model for RF discharges provide ion sources, electron temperature and electric potential. A PIC simulation provides ion–dust momentum transfer cross sections and charges on the dust. A plasma chemistry Monte Carlo simulation provides ion fluxes. A separate model provides the fluid flow field. These results are combined in the dust particle transport model.

The modelling process begins by computing the electrical charges on the dust and the ion–dust momentum transfer cross sections as a function of ion energy and plasma parameters (such as electron density and temperature). These cross sections are obtained from the PICS which follows electron and ion trajectories in the vicinity of a dust particle while solving Poisson's equation for the electric field. Before executing the PICS, Monte Carlo simulations (MCSS) of both the electron and ion swarms are performed using a specified and spatially uniform E/N (electric field/gas number density). The purpose of performing the MCSS is to obtain the quasi-steady state electron energy distribution and ion energy distribution for use as initial conditions in the PICS. The details of the MCSS are described by Weng and Kushner [20]. All pertinent elastic and inelastic collisions of electrons with the neutral gas and ions are included in the MCSS. After the electron and ion energy distributions are obtained, a spherical dust particle is introduced into the centre of the computational volume having a specified charge Q. The PICS is then performed while including all the collision processes. This portion of the model differs from the MCS in that now the self-consistent electric field in the vicinity of the dust particle is obtained by solving Poisson's equation while the equations of motion of the pseudoparticles are advanced. When solving Poisson's equation, the net charge density in the plasma and on the surface of the dust particle are accounted for. The surface charge density provides a boundary condition in the form of the electric field at the surface. Pseudoparticles striking the dust particle are assumed to be collected with unity efficiency. The collected charge density was averaged over the surface of the dust particle. The PICS is executed to obtain dQ/dt. Based on the sign of dQ/dt, the PICS is repeated with difficult values of Q to search for the value of Q which yields $dQ/dt = 0$ which signals an equilibrium of electron and ion fluxes to the dust particle.

At the end of the PICS, cross sections for electron and ion momentum transfer to the dust particle, and for collection by the dust particle are calculated using molecular dynamics (MD) techniques. Given the electric field around the dust particle obtained from the PICS, electron and ion pseudoparticles are launched into the computational volume with varying impact parameters. By gathering statistics on the change in momentum and number of pseudoparticles as they leave the volume, one can calculate the momentum transfer and capture cross sections.

A two-dimensional MCFH model of RF discharges is then used to obtain electric fields as a function of position and source functions for ions and radicals [19]. The two-dimensional (r, z) model is a hybrid simulation consisting of an electron Monte Carlo simulation (EMCS), a fluid-chemical kinetics simulation (FKS), and an off-line plasma chemistry Monte Carlo simulation. The model is conceptually a 2D analogue of the 1D MCFH model for RF discharges described previously [21]. The hybrid model begins by estimating electric fields in the plasma as a function of position and phase $E(r, z, \phi)$.

These fields are used in the EMCS to advance electron trajectories to calculate the time averaged electron energy distribution, $f(\varepsilon, r, z)$. This is obtained by averaging electron trajectories over ≈ 50 RF cycles while including all pertinent elastic, inelastic, and Coulomb collisions [21]. $f(\varepsilon, r, z)$ is then used to calculate source functions for electron impact processes, transport coefficients, and average electron energies as a function of (r, z). These quantities are then passed to the FKS. The FKS integrates the continuity equations for the densities of all charged and neutral species and solves Poisson's equation for the electrostatic plasma potential using the method of successive-over-relaxation. A semi-implicit solution of Poisson's equation allows us to take time steps tens to hundreds of times larger than the dielectric relaxation time if necessary. An acceleration technique is used to speed the convergence of the FKS by predicting future species densities based on recent time histories of those densities [22].

We account for the different effective areas of the electrodes by using a simple circuit having a blocking capacitor, and calculate the DC bias generated on the substrate. The surfaces of the chamber are specified as being either metal or dielectric. We can also include on the substrate topography such as wafers, discs and grooves of specified dielectric constant. After the FKS, $E(r, z, \phi)$ and species densities are cycled back to the EMCS to iterate through the model until the plasma density converges.

In the MCFH model, electrons are treated kinetically while ions are treated as a fluid. We therefore do not generate the information on the ion energy distributions that is required to compute the forces on the dust particles. To obtain these distributions the electric field and source functions from the MCFH model are imported into the PCMCS In the PCMCS, source functions and electric fields from the MCFH are used to launch and follow trajectories of pseudoparticles representing ions and radicals. All pertinent elastic and inelastic collisions for both ions and radicals are included. An iterative particle–mesh algorithm incorporating a modified null cross section technique is used to account for ion–ion (such as negative ion-positive ion neutralization) and radical–radical collisions [23]. Statistics are collected on the velocity and spatially resolved ion momentum flux distribution, $\phi_I(r, z, v_I)$[g/(cm^{2}s^{-1})/(cm s^{-1})].

The fluid flow field in the reactor is obtained by solving the perturbative pressure form of the continuity and momentum equations.

$$\frac{\partial \boldsymbol{u}}{\partial t} = -\nabla \cdot \boldsymbol{u}\boldsymbol{u} - \frac{\nabla \rho'}{\rho_0} - D\nabla^2 \boldsymbol{u} \tag{1a}$$

$$\frac{\partial \rho'}{\partial t} = -\rho_0 c_0^2 \nabla \cdot \boldsymbol{u}. \tag{1b}$$

In equation (1) $\boldsymbol{u}$ is the advective fluid velocity, ρ' is the perturbative pressure, ρ_0 is the gas density, c_0 is the sound speed and D is the velocity diffusion coefficient. This flow field is also used in the PCMCS to account for momentum transfer between the pseudoparticles and buffer gases during elastic collisions.

The motions of the dust particles are calculated in the DPT model where we compute the spatially dependent ($\boldsymbol{r} = (r, z)$) forces on the dust particles. To obtain these forces we import the ion–momentum transfer cross sections and dust charges (from the PICS), electric fields (from the MCFH model), ion momentum distributions (from the PCMCS model) and the fluid flow field. For this work we have simply specified a temperature gradient. The force on a dust particle i having a specified radius r_i and mass M_i is

$$\boldsymbol{F}_i(\boldsymbol{r}) = M_i\boldsymbol{g} + q_i\boldsymbol{E} + \int \sigma(|v_I|)\phi_I(r, v_I)|v_I|\,\mathrm{d}v_I - \frac{6\pi\mu r}{C(Kn)}(\boldsymbol{v}_i - \boldsymbol{u}) \cdot C_D(Re_p)\frac{Re_p}{24} - 6\pi\mu r_i \nu K_T \cdot \frac{\nabla T}{T}. \tag{2}$$

The terms on the right-hand side of equation (2) are for gravitational, electrostatic forces, ion drag, viscous fluid drag and thermophoretic forces respectively. $\boldsymbol{E}$ is the electric field (obtained from the MCFH model), q_i is the charge on the dust particle (obtained from the PICS), σ is the ion–momentum transfer cross section (obtained from the PICS) and ϕ is the ion momentum flux distribution (obtained from the MCPC model). The last two terms, viscous fluid drag and thermophoretic forces, are derived from classical thermodynamics based on the hard sphere particle assumption [17, 24]. The constants are

$$C(Kn) = 1 + Kn(\alpha + \beta) \cdot \exp\left(-\frac{\gamma}{Kn}\right) \tag{3a}$$

$$C_D(Re_p)\frac{Re_p}{24} = 1 + 0.173 \cdot Re_p^{0.657} + \frac{0.01721 \cdot Re_p}{1 + 16300 \cdot Re_p^{-1.09}} \tag{3b}$$

$$Re_p = \frac{2\rho r_i |\boldsymbol{v}_i - \boldsymbol{u}|}{\mu} \tag{3c}$$

$$K_T = \frac{2C_s[(k_g/k_p) + C_t Kn]}{(1 + 3C_m Kn)[1 + 2 \cdot (k_g/k_p) + 2C_t Kn]}. \tag{3d}$$

v_i is the velocity of the dust particle, Kn is the Knudsen number (λ/r_i), Re_p is the Reynolds number, μ is the fluid viscosity, $\nu = \mu/\rho$ (ρ is the gas density), and T is the mean gas temperature. In equation (3) α, β and γ are experimental constants which depend on the nature of the gas–particle interaction at the particle surface and so are affected by both gas composition and particle surface roughness. k_g and k_p are the gas and particle thermal conductivities respectively, and C_t, C_s, and C_m are the thermal creep coefficient, temperature jump coefficient, and velocity jump coefficient respectively. All values of the constants in equation (3) are listed in table 1.

To begin the DPT model, we specify a volumetric rate of generation of dust particles of a given radius. We then launch pseudoparticles representing the dust particles from those locations, and simply integrate the equations of motion of those pseudoparticles while continuously

Table 1. Values of constants used in force calculations

Constant	Value	Reference
α	1.227	[24]
β	0.42	[24]
γ	0.85	[24]
k_g	$0.1799\,mW\,cm^{-1}K^{-1}$	[28]
k_p	$1240\,mW\,cm^{-1}K^{-1}$	[28]
C_t	2.2	[24]
C_s	1.147	[24]
C_m	1.146	[24]

launching additional pseudoparticles until the dust distribution achieves a steady state.

3. Distribution of dust particles

In this work we investigated dust particle distributions in a capacitively coupled RF (13.56 MHz) discharge sustained in 100 mTorr of argon with a nominal power deposition of $\simeq$20–200 W (see figure 2). The electrodes are separated by 3 cm and the plasma zone is 10 cm in diameter. The gas flows through a showerhead nozzle and out radially to a pump port (figure 3). A wafer (dielectric constant $\varepsilon/\varepsilon_0 = 11.8$, thickness 3 mm) sits on the lower powered electrode. The top electrode is grounded. The radial boundary condition is approximated as a ground plane (at $r = 10$ cm) which allows the advective flow to pass. For these results we have assumed a constant thermal gradient of $15\,K\,cm^{-1}$ as

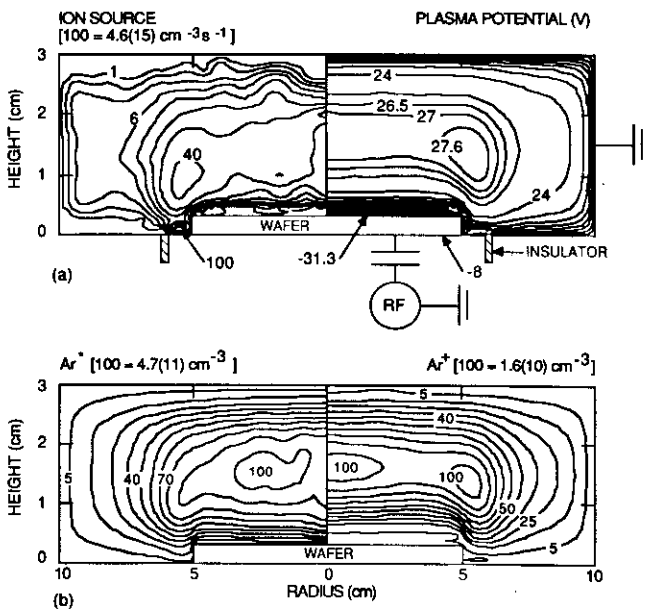

Figure 2. Plasma parameters from the MCFH model for a capacitively coupled RF discharge (13.56 MHz) in 100 mTorr Ar (*a*) ion source and plasma potential. (*b*) Ar(4s) and Ar^+ densities. The contour labels for ion source and densities are a percentage of the maximum value, noted at the top of the figure. A 3 mm thick wafer (10 cm diameter) is on the lower powered electrode. The electrode topography produces a local maximum in the plasma potential and the ion source.

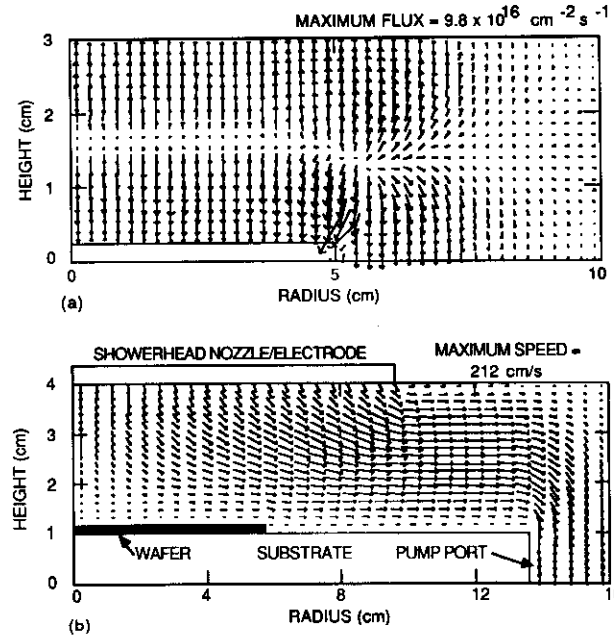

Figure 3. Flow fields for the condition of figure 2. (*a*) Ion flux and (*b*) advective fluid velocity. The size of the arrow denotes the magnitude of the ion flux or fluid velocity. The maximum value is shown at top. The ion flux moves away from the local maxima in ion source and plasma potential to the boundaries. The fluid velocity is most negative at the showerhead nozzle and is almost totally radial near the edge of the wafer.

could occur when actively cooling the wafer. We observe that the calculated thermophoretic force is smaller than the electrostatic or ion drag forces, and therefore is not a major consideration under our operating conditions.

Typical results from the MCFH models are given in figure 2 where the time averaged plasma potential, ion source, ion density and argon metastable density are shown. A 10 cm diameter wafer is placed on the powered electrode. The powered diameter of the lower surface is $\simeq$12 cm and is separated from the annular ground plane by a dielectric spacer. The metal surface of the powered electrode generates a DC bias of -8 V, while the surface of the wafer aquires a DC bias of -31 V. Note that there are local maxima in the plasma potential, electron sources and ion density in the form of a toroidal ring 1–1.5 cm from the edge of the wafer.

The positive potential well has a depth of $\simeq$1–1.5 V. These local maxima, perhaps similar to those observed by Geha *et al* [18], result from a discontinuity in the electrical topography produced by the sharp edge of the wafer, and by the transition between the dielectric wafer and the metal. In this regard, the discontinuity in electrode topography resembles the metal–gas–dielectric triple point at which electric field enhancement occurs in high-voltage switches [25]. The ion density shows a small maximum in this toroidal region as well as at the centre of the plasma. The Ar(4s) density also shows a weak off-axis peak. Note that although the ion source has a local maximum near the edge of the wafer, its absolute maximum value is near the exposed

powered electrode. This results from the fact that the full capacitive voltage drop is across the sheath as opposed to sharing the voltage between the wafer and the sheath.

The ion flux (obtained from the PCMCS) and fluid flow fields for these conditions are shown in figure 3. The ion flux typically flows from maxima in the plasma potential and ion sources to the peripheries of the reactor. The local maxima in the plasma potential and ion source at the edge of the wafer produces a vertex in the ion flux with ions flowing from that location. The fluid flow starts from the showerhead and gains speed in the radial direction as the edge of the showerhead is approached.

Predictions of dust particle locations for dust diameters of 0.5 to 4 μm are shown in figure 4 for the geometry just discussed. These results are an instantaneous 'snapshot' of the dust particle locations 0.15 s after beginning to generate particles. The dust particles are generated at a constant rate of $2.6 \times 10^4\,s^{-1}$ in the plasma region of the reactor weighted by a cosine (maximum in the centre) in both the axial and radial directions. The power is 80 W and the gas flow is turned off. The smaller sized particles are trapped near the centre plane of the reactor at the maximum in the plasma potential. The dust particles are also trapped around, but not in, the positive potential well. Ion flux flowing out of the well is fairly efficient at removing particles from that region and holding them at the periphery. We also observe that the plasma optical emission and particle locations do not necessarily coincide. Trapped particles follow a contour on which ion drag and electrostatic forces balance. This contour moves down towards the edge of the wafer around both sides of the local maximum in potential on both sides. These loci of points forming the trapping locations give the appearance of a 'dome' above the wafer and 'ring' around the wafer as observed experimentally by others [2, 26, 27] at a similar power deposition value ($240\,mW\,cm^{-2}$).

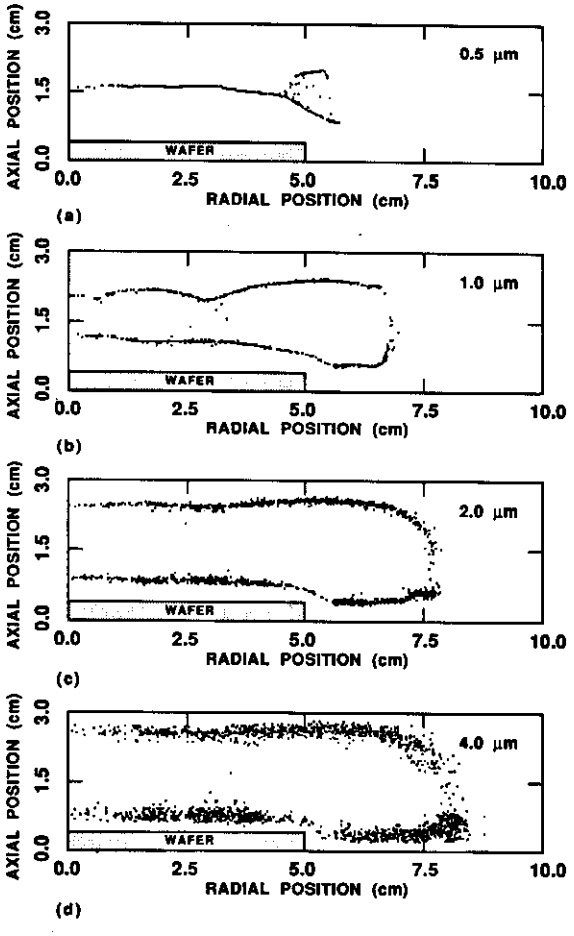

Figure 4. Dust particle locations with a 10 cm diameter wafer on the powered electrode. Locations are shown for (*a*) 0.5, (*b*) 1.0, (*c*) 2.0 and (*d*) 4.0 μm particles. Small particles are more sensitive to the electric potential and may form domes and rings around local maxima in the potential caused by ion drag away from those locations. Large particles have larger ion drag forces, which push them towards the boundaries. Inertial effects cause oscillation about the equilibrium locations.

As the particle size increases, the trapping location moves toward the electrodes and a flatter dome and a wider ring form. The ion drag force increases at a faster rate with increasing particle size than does the electrostatic force, and so the large particles are pushed by the ions towards the periphery. The ion drag forces are sufficiently large for particles $\geqslant 2$–4 μm that inertial effects are important. That is, the dust particles are accelerated to high velocities which overshoot the equilibrium location at which ion drag and electrostatic forces are balanced. The particles therefore oscillate about those locations as their velocities are slowly damped by fluid drag forces. The oscillation is shown by the 'blurring' of the particle locations in the snapshot of figure 4(*d*). Although we collect all particles striking the electrodes, many of the larger particles strike the electrodes and could conceivably bounce off the surface.

Particle locations are shown in figure 5 (1 μm diameter) for similar conditions as in figure 4 except for a 15 cm diameter wafer on the powered electrode and power deposition of 20–240 W. The largest difference which occurs with increasing power deposition is an increase in the ion flux while the potential profile does not change appreciably. As with the smaller wafer, there is a local maximum in the plasma potential and ion flux near the edge of the wafer as shown in figure 6. But now with the larger wafer, there is also a maximum in the plasma potential at the centre of the wafer. At low-power deposition, the electrostatic forces dominate, and the particles accumulate at the ridge the maximum in the plasma potential. As the power increases and ion drag forces increase, the particles are pushed away from the maximum in the plasma potential, and form ring- and dome-like structures. These locations are on opposite sides of the maximum in the plasma potential where the ion drag caused by ions flowing away from the maximum is balanced by electrostatic forces. As the power continues to increase, the ion drag forces dominate and push the particles to the sheaths at the edge of the wafer. At high powers, the ion drag forces accelerate the dust particles to sufficiently high velocities that they overshoot the equilibrium location. Evidence of oscilla-

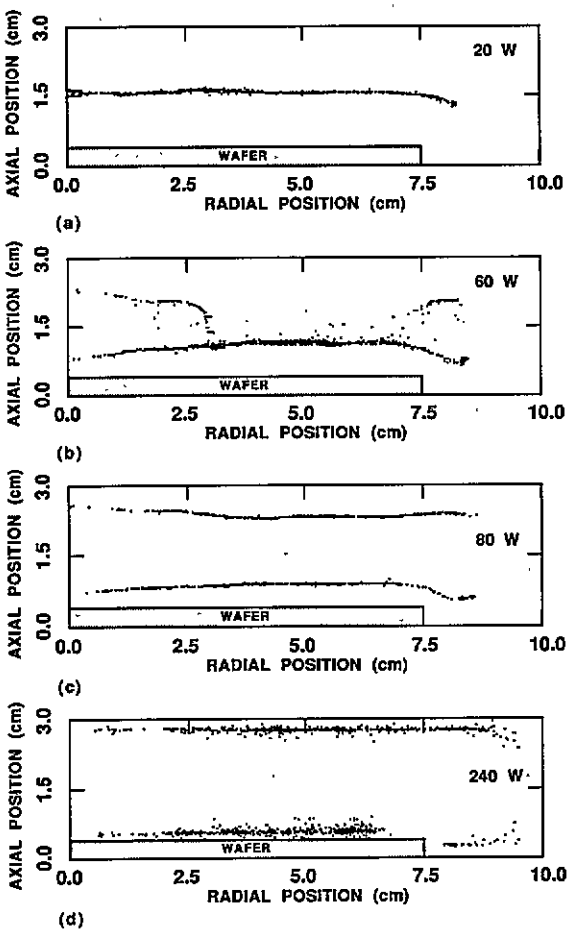

Figure 5. Dust particle (1 μm) locations with a 15 cm diameter wafer on the powered electrode. Locations are shown for power depositions of (*a*) 20, (*b*) 60, (*c*) 80 and (*d*) 240 W. Increasing power increases the ion drag force, pushing particles towards the electrodes. The dome and ring structures result from local maxima in the plasma potential.

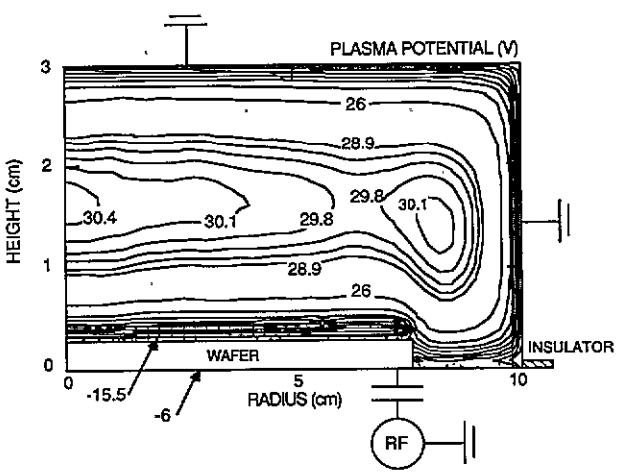

Figure 6. Plasma potential for the conditions of figure 5 (20 W). The dots denote regions of negative potential. Maxima in plasma potential occur near the edge of the wafer and in the centre of the reactor.

tion in the location of the particles can be seen by the 'blurred' line of particles. These predictions agree with the experimental observations of Selwyn *et al* [26] who noted that particle traps can be emptied by increasing power deposition, an effect we attribute to an increased component of ion drag.

The effects of gas flow on trapping are shown in figure 7 for 1 μm particles and a power deposition of 80 W. Note that no wafer is used in this sequence where we varied the gas flow from zero to 500 sccm. Without gas flow, the particles are trapped at the sheath edges where electrostatic and ion drag forces balance. As the gas flow increases the particle trap near the top grounded electrode is eliminated by the fluid forces. At this location the fluid drag force is negative (towards the lower electrode) and opposes the ion drag which forces the particles towards the upper electrode (see figure 3). With increasing gas flow particles are swept in the radial direction where they are lost out of the gas outlet and accumulate to some degree at the radial sheath. This accumulation may be exaggerated by our electrical radial boundary condition. At very high gas flow, the inertia imparted to the particles by the high axial gas flow near the showerhead causes particles to oscillate about equilibrium trapping points.

The disposition of 1 μm particles is shown in figure 8 where the normalized rates of loss of particles to traps,

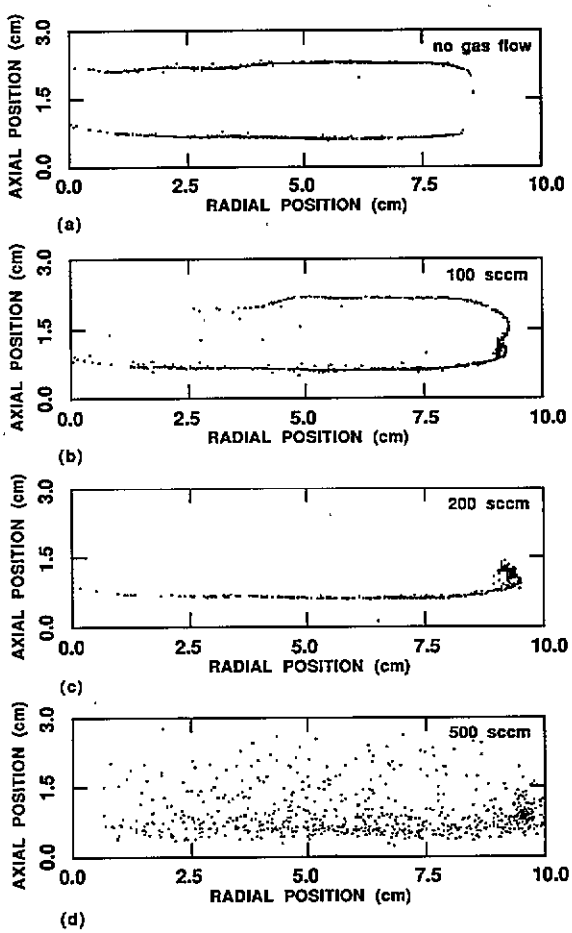

Figure 7. Dust particle locations with a bare powered electrode. Locations are shown for (*a*) 0, (*b*) 100, (*c*) 200 and (*d*) 500 sccm of gas flow. The gas flow detraps particles at the upper boundary where the fluid velocity is negative and opposes the ion drag forces. Particles are lost via the radial pump port at high gas flow.

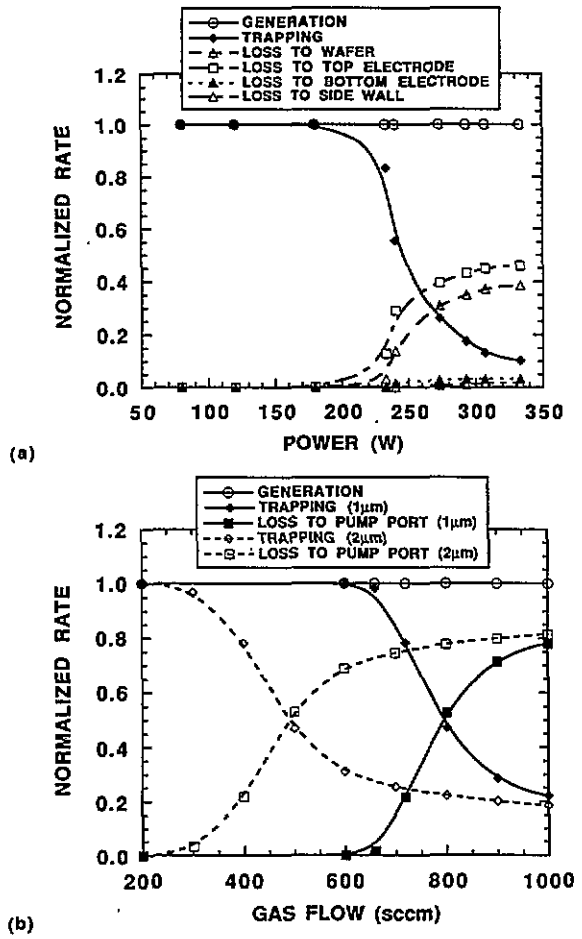

Figure 8. Disposition of particles as a function of (*a*) power deposition (1 μm diameter) and (*b*) gas flow (1 and 2 μm diameter). Rates of trapping and loss to the wafer, bottom electrode (but not the wafer), top electrode and to the side wall or gas outlet are shown.

the top electrode, the bottom electrode (but not the wafer), the wafer and to the side wall (or out the pump port) are shown. Results are presented as a function of power deposition (without gas flow) and gas flow (at 80 W). In the low-power regime and without gas flow, most particles are trapped in the plasma. As the power increases the trapping rate decreases and the particle loss to the reactor boundaries increases. This results from ion drag forcing particles over the potential hill at the boundaries. At 300 W (without gas flow), only 10% of the particles are trapped. Note that the rate of loss of particles to the wafer is smaller than to the top electrode because of its more negative sheath (and smaller size). The particle dispositions as a function of gas flow show that at sufficiently high gas flows, the particles can be blown out of the pump port. Larger particles are more easily blown out of the reactor because both the fluid drag and ion drag forces increase with radius of the dust particle. These results are sensitive to the starting locations of the dust particles.

The interplay between electrostatic, ion drag and fluid forces ultimately determines the disposition of the particles. This interplay is illustrated in figure 9 where particle locations are shown when a metal washer is placed on the lower electrode. The gas flow is 200 sccm

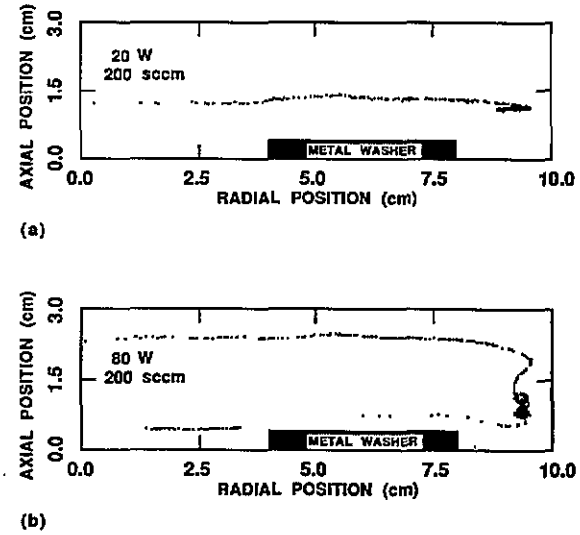

Figure 9. Particle traps are shown when a metal washer is placed on the powered electrode for a gas flow of 200 sccm with (*a*) 20 W and (*b*) 80 W of power deposition. With the higher power particles are trapped on the inside of the wafer where an axial potential well exists.

and results are shown for 20 and 80 W power deposition. The sheath follows the contours of the washer, thereby creating a potential well with respect to axial location in the centre of the washer. At the lower powers, 1 μm particles are trapped in a flat dome above the wafer and are blown towards the radial boundary. When the power is increased to 80 W, the particles are pushed by ion drag to the electrodes. Some particles, which are generated in the centre of the reactor, are trapped inside the washer. The particles inside the washer do not have enough energy to climb the electrostatic potential barrier over the washer and exit through the gas outlet. The gas flow inside the washer has no appreciable radial component to push the particles out of the centre of the ring.

4. Concluding remarks

A series of linked computer models has been developed and used to investigate the trapping of dust particles in capacitively coupled RF discharges with various electrode topographies. Lower rates of wafer contamination are obtained at low-power deposition where particles are allowed to be trapped in the gas phase, and high gas flow where the particles are blown towards the pump ports. At higher power deposition, ion drag forces dominate and particles are pushed through the sheaths to the boundaries. Various shapes of particle trapping locations are formed under different operating conditions. At low powers, we observed both 'dome' and 'ring' types of particle traps as seen experimentally [3, 26, 27] which result from a balance of ion drag and electrostatic forces generated by perturbations in these quantities caused by local extrema in the ion generation and potential, ultimately caused by electrode topography. At high power or high gas flow, the dust particles can gain sufficient

inertia that they will oscillate about the equilibrium trapping locations, or climb potential hills of tens of volts to reach the substrate.

5. Acknowledgments

We thank D Rader, A Geller, M Barnes, G Selwyn, J Goree, J Keller and D Graves for their advice and discussions on dusty plasmas. This work was supported by the National Science Foundation (CTS 91-13215 and ECS 91-09326), Sandia National Laboratory, the Semiconductor Research Corporation and the University of Wisconsin ERC for Plasma Aided Manufacturing.

References

[1] Roth R M, Spears K G, Stein G D and Wong G 1985 *Appl. Phys. Lett.* **46** 235
[2] Selwyn G S, Heidenreich J E and Haller K L 1990 *Appl. Phys. Lett.* **57** 1876
[3] Selwyn G S, Singh J and Bennett R S 1989 *J. Vac. Sci. Technol.* A 7 2758
[4] Selwyn G S, McKillop J S, Haller K L and Wu J J 1990 *J. Vac. Sci. Technol.* A **8** 1726
[5] Jellum G M and Graves D B 1990 *Appl. Phys. Lett.* **57** 2077
[6] Jellum G M and Graves D B 1990 *J. Appl. Phys.* **67** 6490
[7] Jellum G M, Daugherty J E and Graves D B 1991 *J. Appl. Phys.* **69** 6923
[8] Watanabe Y, Shiratani M and Makino H 1990 *Appl. Phys. Lett.* **57** 1616
[9] Watanabe Y, Shiratani M and Yamashita M 1992 *Appl. Phys. Lett.* **61** 1510
[10] Carlile R N, Geha S G, O'Hanlon J and Stewart J 1991 *Appl. Phys. Lett.* **59** 1167
[11] Choi S J and Kushner M J 1995 *Appl. Phys. Lett.* **62** 2197
[12] Choi S J and Kushner M J 1994 *IEEE Trans. Plasma Sci.* to be published
[13] Sommerer T J, Barnes M S, Keller J H, McCaughey M J and Kushner M J 1991 *Appl. Phys. Lett.* **59** 638
[14] Barnes M S, Keller J H, Forster J C, O'Neill J A and Coultas D K 1992 *Phys. Rev. Lett.* **68** 313
[15] Daugherty J E, Porteous R K and Graves D B 1993 *J. Appl. Phys.* **73** 1617
[16] Kilgore M D, Daugherty J E, Porteous R K and Graves D B 1993 *J. Appl. Phys.* **73** 7195
[17] Talbot L, Cheng R K, Schefer R W and Willis D R 1980 *J. Fluid Mech.* **101** 737
[18] Geha S G, Carlile R N, O'Hanlon J F and Selwyn G S 1992 *J. Appl. Phys.* **72** 374
[19] Ventzek P L G, Sommerer T J, Hoekstra R J and Kushner M J 1993 *Appl. Phys. Lett.* **63** 605
[20] Weng Y and Kushner M J 1992 *Phys. Rev.* A **42** 6192
[21] Sommerer T J and Kushner M J 1992 *J. Appl. Phys.* **71** 1654
[22] Pak H and Riley M 1992 *Proc. 45th Gaseous Electronics Conference (Boston MA) 1992* Unpublished, paper BB-5
[23] Hartig M J and Kushner M J 1993 *Appl. Phys. Lett.* **62** 1594
[24] Rader D J 1994 Plasma Sources Sci. Technol. **3** 426
[25] Gradinaru G and Sudarshan T S 1993 *J. Appl. Phys.* **73** 7643
[26] Selwyn G S, Heindenreich J E and Haller K L 1991 *J. Vac. Sci. Technol.* A **9** 2817
[27] Selwyn G S 1991 *J. Vac. Sci. Technol.* B **9** 3487
[28] Weast R C, Lide D R, Astle M J and Beyer W H (eds) 1989 *CRC Handbook of Chemistry and Physics* (Boca Raton, FL: CRC)